

# Characterizing the Low-Frequency QPO behavior of the X-ray Nova XTE J1550–564

Gregory J. Sobczak<sup>1</sup>, Ronald A. Remillard<sup>2</sup>, Michael P. Muno<sup>2</sup>, Jeffrey E. McClintock<sup>3</sup>

Received \_\_\_\_\_; accepted \_\_\_\_\_

arXiv:astro-ph/0004215v1 15 Apr 2000

---

<sup>1</sup>Harvard University, Astronomy Dept., 60 Garden St. MS-10, Cambridge, MA 02138;  
gsobczak@cfa.harvard.edu

<sup>2</sup>Center for Space Research, MIT, Cambridge, MA 02139; rr@space.mit.edu,  
muno@space.mit.edu

<sup>3</sup>Harvard-Smithsonian Center for Astrophysics, 60 Garden St. MS-3, Cambridge, MA  
02138; jem@cfa.harvard.edu

## ABSTRACT

For all 209 RXTE observations of the 7-Crab X-ray nova XTE J1550–564, we analyzed the X-ray power spectra, phase lags, and coherence functions. These observations cover the entire 250 day outburst cycle of the source and are the most complete and arguably the richest data set for any black hole X-ray nova. We find that there are three fundamental types of QPO behavior—one more than reported by Wijnands, Homan, & van der Klis (1999, ApJ, 526, 33). The new type occurred during the first half of the outburst. These three types of QPO behavior can be grouped according to the relative contributions of the disk and power-law components to the total flux.

*Subject headings:* black hole physics — stars: individual (XTE J1550-564) — X-rays: stars

## 1. Introduction

XTE J1550–564 is an X-ray nova and black hole candidate discovered with the All Sky Monitor (ASM; Levine et al. 1996) onboard the *Rossi X-ray Timing Explorer* (RXTE) in 1998 September (Smith et al. 1998). The outburst lasted until 1999 May; its duration was approximately 250 days, during which time RXTE performed an almost daily series of pointed observations. A summary of these observations can be found in Sobczak et al. (2000b). Extensive spectral and timing studies of this source have been performed using these data. The source has been observed in the very high, intermediate, and high/soft outburst states of black hole X-ray novae, with an X-ray spectrum that can be well modeled by multicolor blackbody disk and power-law components (Sobczak et al. 1999,2000b; Homan et al. 2000).

The power spectra of XTE J1550–564 exhibit quasiperiodic X-ray oscillations (QPOs) at both high frequencies ( $\sim 100$ –285 Hz) and low frequencies (0.08–18 Hz) (Remillard et al. 1999; Sobczak et al. 1999; Cui et al. 1999; Homan et al. 2000). Herein we are interested only in the latter ‘low-frequency’ QPOs. These QPOs can have large amplitudes, with peak to trough ratios as high as 1.5 (Remillard et al. 1999), which indicates that they are a fundamental aspect of the accretion process. A sample lightcurve of XTE J1550–564 can be seen in Figure 1 of Sobczak et al. (2000a), which explored the correlations between the QPO frequency and amplitude and the X-ray spectral parameters. They reported that both the power-law and the disk components are linked to the QPO phenomenon: QPOs are observed only when the power-law component contributes more than 20% of the 2–20 keV flux, and the QPO frequency generally increases as the disk flux increases.

Our focus in this paper is on the properties of the phase lags associated with the low-frequency QPOs. The Fourier time delay, or lag, can be computed to measure the phase lags between soft and hard X-ray energy bands. Recent studies have shown that the phase

lags associated with low-frequency QPOs and their harmonics are quite complex. In one observation of GRS 1915+105, Cui (1999) found that the lower energy (soft) photons lagged behind the higher energy (hard) photons (“soft lag”) for the fundamental QPO and its 2nd harmonic; however, the higher energy photons lagged behind the lower energy photons (“hard lag”) for the 1st and 3rd harmonics. Wijnands, Homan, & van der Klis (1999) reported even more complicated behavior from 14 observations of XTE J1550–564 near the end of the outburst. However, Wijnands et al. were able to show that the complicated phase lag behavior observed in these 14 observations actually consists of variations on only two fundamental types. Phase lags for 13 observations during the initial rise of XTE J1550–564 are discussed by Cui, Zhang, & Chen (2000).

In this paper we analyze the phase lags for all 209 RXTE observations of XTE J1550–564. These observations cover the entire 250 day outburst cycle of the source and are the most complete and arguably the richest data set for any black hole X-ray nova. We find that there are three fundamental types of phase lag behavior – one more than reported by Wijnands et al. (1999). The new type occurred during the first half of the outburst. We discuss correlations between the phase lags and the X-ray spectral parameters, QPO frequencies, and amplitudes.

## 2. Observations and Data Analysis

The PCA data were accumulated with  $125\mu\text{s}$  resolution in ‘single bit’ mode, providing two energy channels corresponding roughly to 2–6 and 5–13 keV (modes SB\_125us\_0\_17\_1s & SB\_125us\_18\_35\_1s), respectively. Above 13 keV, the event mode was used with 16 energy channels and  $16\mu\text{s}$  time resolution (mode E\_16us\_16B\_36\_1s). The single bit data modes were combined into a single channel, resulting effectively in two energy channels covering 2–13 keV and 13–30 keV (which corresponds to PCA channels 0–35 and 36–255,

respectively). These three data modes and channels ranges were not available for five of the observations listed in Table 1. The alternate channel ranges for those observations are given in the footnotes to Table 1.

We compute the phase lag between the two energy bands as follows (Bendat & Piersol 1986; Cui et al. 1997; Vaughan & Nowak 1997). Let  $a(t)$  &  $b(t)$  denote the lightcurves in two energy bands with Fourier transforms  $A(f)$  &  $B(f)$ . The cross spectral density or cross power spectrum is given by

$$C(f) = \langle A^*(f)B(f) \rangle, \quad (1)$$

where  $\langle \rangle$  denotes an average over an ensemble of measurements. If  $R(f)$  and  $I(f)$  are the real and imaginary parts of  $C(f)$ , then the average phase lag of  $b(t)$  with respect to  $a(t)$  is

$$\Delta\phi(f) = \tan^{-1} \left( \frac{I(f)}{R(f)} \right), \quad (2)$$

It follows that the time lag of  $b(t)$  with respect to  $a(t)$  is  $\Delta t = \Delta\phi/2\pi f$ .

The coherence function,  $\gamma^2(f)$ , is a measure of the linear correlation between two simultaneous time series as a function of frequency and is defined by

$$\gamma^2(f) = \frac{|\langle C(f) \rangle|^2}{\langle |A(f)|^2 \rangle \langle |B(f)|^2 \rangle} \quad (3)$$

(Bendat & Piersol 1986; Vaughan & Nowak 1997; Nowak et al. 1999). The coherence functions reported here include a correction for the effects of Poisson noise and were calculated using equation (8) in Vaughan & Nowak (1997). If the coherence is significantly less than unity then the measured phase lag cannot be trusted.

See Remillard et al. (1999) and Sobczak et al. (2000a) for information regarding the analysis of the power density spectra (PDS) for XTE J1550–564. The QPO properties for each observation are listed here in Table 1.

### 3. Results

We find three fundamental types of phase lag behavior for XTE J1550–564 – one more than the two types identified by Wijnands et al. (1999). Figures 1–4 show representative power density spectra, phase lags, and coherence functions for these three types of timing behavior. Types A and B correspond to those identified previously by Wijnands et al. Type C, the third type of phase lag behavior, appears during the first half of the outburst that was not analyzed by Wijnands et al. Figure 6 shows that these three types of QPO behavior can be grouped according to the relative contribution of the disk (or power-law) component to the total flux. The characteristics of each type of QPO behavior are discussed below and summarized in Table 2.

Type A timing behavior is characterized by broad QPO features in the PDS ( $Q \sim 2\text{--}3$ , where  $Q = \nu/\Delta\nu$ ) near 6 Hz that are likely the superposition of a QPO peak and its harmonic (Fig. 1). The integrated rms amplitude of the QPO features is a few percent. The phase lags for type A behavior are generally featureless except for a broad soft lag centered near the QPO feature with  $|\Delta\phi| \sim 1$  rad and poor coherence ( $< 50\%$ ). The soft spectral component from the accretion disk contributes  $\sim 50\text{--}70\%$  of the 2–20 keV flux during type A behavior (Fig. 6). We identify 4 observations with type A QPO behavior, all of which display high-frequency ( $\nu \sim 100\text{--}284$  Hz) QPOs (Remillard et al. 1999; Homan et al. 2000; Remillard, private communication).

Type B timing behavior is characterized by a narrow fundamental QPO feature ( $Q \sim 10$ ) at 5–6 Hz (Fig. 2) with rms amplitude  $\sim 4\%$ . The first and sub-harmonic of the fundamental QPO feature are also apparent at 11–12 and 2.5–3 Hz, respectively. Type B observations display a hard lag nearly coincident with, but slightly off-center from, the fundamental QPO feature with  $\Delta\phi \sim 0.0\text{--}0.4$  rad, as well as soft lags associated with the first and sub-harmonics. The coherence of the type B fundamental lags is typically within

10% of unity and has small statistical errors, but the coherences of the harmonics have large errors. Type B timing behavior is observed when the power-law component contributes 60–75% of the 2–20 keV flux (Figure 6). We identify 9 observations with type B QPO behavior, all of which display high-frequency QPOs.

We now introduce type C timing behavior (Fig. 3), which occurs primarily during the first half of the outburst when the source is in the very high state and the power-law component contributes  $\gtrsim 75\%$  of the 2–20 keV flux (Figure 6). Type C timing behavior is characterized by sharp ( $Q \gtrsim 10$ ) fundamental QPO features with a range of rms amplitudes from 3–16%. The first harmonic is present, and the first sub-harmonic is usually observed as well. The phase lags for type C behavior are typically modest, with the fundamental exhibiting soft lags  $|\Delta\phi| \lesssim 0.4$  rad. The sub-harmonic usually has a small soft phase lag of the same magnitude as the fundamental, whereas, the first harmonic has a hard lag, which can be several times larger than the soft lag displayed by the fundamental. The coherence of the fundamental lag is high  $\sim 85\text{--}95\%$ , while the coherence of the first and sub-harmonic are typically closer to 75–80%. We identify 50 observations with type C QPO behavior, only three of which also display high-frequency QPOs (observations 17 & 18 on 1998 September 20 and observation 161 on 1999 March 13; see Table 1).

The 50 type C observations can be further subdivided into 45 type C<sub>1</sub> and 5 type C<sub>2</sub> classifications. In the five type C<sub>2</sub> observations (Fig. 4 and open circles in Fig. 6), the fundamental QPO appears to be a superposition of two narrow QPO features and the harmonics are difficult to discern. By dividing the observations into smaller time increments, we found that this blended QPO feature is the result of a single QPO with a centroid frequency that varies during the observation. The five type C<sub>2</sub> observations all occurred during the two days (1998 September 20–21) immediately following the 6.8 Crab flare in the XTE J1550–564 lightcurve. The fundamental type C<sub>2</sub> QPOs have frequencies

from 6–10 Hz with rms amplitudes of 3–7% and phase lags of  $\sim -0.2$  rad. When we make the distinction between types C<sub>1</sub> and C<sub>2</sub> QPOs, Figure 7a shows that the frequency of type C<sub>1</sub> QPOs increases nearly linearly with the 2–20 keV disk flux. Two of the three type C observations that display high-frequency QPOs belong to the C<sub>2</sub> subgroup.

There are two exceptions to the three fundamental types of QPO behavior described above. The first anomalous QPO occurred during the 6.8 Crab flare on 19 September 1998 (Sobczak et al. 1999; Remillard et al. 1999). The PDS for this observation shows a 13 Hz QPO with an integrated rms amplitude of 1% (Fig. 5). The QPO has a large soft lag of  $-0.9 \pm 0.2$  rad with a coherence of  $80 \pm 20\%$ . The power-law dominates the spectrum during this flare, with the disk contributing only  $\sim 3\%$  of the 2–20 keV flux. This observation is also the first occurrence of the high-frequency ( $\sim 183$  Hz) QPO. The magnitude of the soft lag and the presence of a high-frequency QPO are consistent with type A behavior, but the QPO frequency and the low contribution of the disk to the total flux for this observation (Fig. 6) are similar to type C behavior.

The second anomalous QPO occurred on 2 March 1999. This QPO is observed at a much higher frequency than the others (18 Hz with an indeterminate phase lag and coherence) with no harmonics. It is significantly sharper than the other QPOs ( $Q \sim 18$ ) and has a very small rms amplitude (0.5%). The disk component contributed 80% of the 2–20 keV flux during this observation.

The three types of QPOs are clearly distinguished by the relative contribution of the disk component to the total flux (Fig. 6). However, most of the observations for which the disk fraction exceeds 0.4 do not exhibit QPOs. Furthermore, no QPOs have been detected when the disk fraction exceeds 0.8.

The phase lag of the fundamental QPO is plotted vs. frequency and amplitude in Figures 8a & 8b for all the QPO types discussed above.

#### 4. Discussion

Hard lags in broadband X-ray lightcurves are often attributed to the Compton upscattering of photons by hot electrons in an extended corona (Miyamoto et al. 1988; Hua & Titarchuk 1996; Kazanas, Hua & Titarchuk 1997; Böttcher & Liang 1998; see also Cui 1999 and references therein). In this scenario, the hard photons undergo more scatterings in order to reach higher energies and therefore lag behind the soft photons. The hard lag is directly related to the photon diffusion time scale through the corona, which scales logarithmically with photon energy (Hua & Titarchuk 1996), in agreement with observations (Cui et al. 1997; Nowak et al. 1999). The time lags reported herein for XTE J1550–564 are typically on the order of 0.001–0.01 s; for a  $10 M_{\odot}$  black hole this corresponds to the light crossing time over 10–100 Schwarzschild radii. However, the measured lags in other sources can be much larger (e.g.  $\sim 1$  s for the 67 mHz (14.9 s) QPO in GRS 1915+105 reported by Cui 1999), which would require an extended Comptonizing region that would be difficult to maintain physically (Nowak et al. 1999; Böttcher & Liang 1999; Poutanen & Fabian 1999). Other models for hard lags include the intrinsic spectral hardening of X-ray emitting magnetic flares (Poutanen & Fabian 1999) and waves or blobs of matter moving inward through an increasingly hotter region where the hard X-rays are emitted (Böttcher & Liang 1999). All of these models have been proposed to explain broadband (continuum) hard lags and do not apply directly to the QPO phenomenon. Furthermore, these scenarios cannot explain the observed soft lags, which may be due to the evolution of the QPO waveform with time (Cui 1999). In addition, both type B & C QPOs exhibit near-perfect coherence, which presents a challenge for QPO models because there are more mechanisms for destroying coherence than there are for producing coherence (Vaughan & Nowak 1997).

High-frequency QPOs are coincident with all types A and B low-frequency QPOs. The

low-frequency QPOs are observed at 5–6 Hz in these cases, whereas the high-frequency QPOs vary in the range 120–285 Hz. This pattern indicates substantially less correlation between the high and low-frequency QPOs in black hole sources than that reported for the corresponding oscillations for accreting neutron stars (van der Klis et al. 1996; Ford & van der Klis 1998; Markwardt, Strohmayer, & Swank 1999). In this sense, the behavior of XTE J1550–564 does not support the idea that QPOs in neutron star and black hole systems are fundamentally related (Psaltis, Belloni, & van der Klis 1999).

We do not include a discussion of the models pertaining to the origin of the QPO phenomenon. The reason for this omission is that none of the models proposed to date contain sufficient detail to fit the observed QPO properties discussed here. See Cui (1999), Markwardt, Swank, & Taam (1999), and Sobczak et al. (2000a) for a discussion of QPO models.

## 5. Conclusions

In conclusion, we summarize the observed QPO properties for XTE J1550–564. First, whenever QPOs are observed the power-law component contributes more than 20% of the 2–20 keV flux (Sobczak et al. 2000a). During the very high state of the outburst, when the QPOs have the largest amplitude, the disk component contributes as little as 3% of 2–20 keV flux (Sobczak et al. 1999,2000b). However, the QPO frequency generally increases as the disk flux increases (Fig. 7a). These results demonstrate that both the disk and the power-law components are linked to the QPO phenomenon. Secondly, there are three fundamental types of QPO behavior which can be grouped according to the relative contributions of the disk and power-law components to the total flux (Fig. 6). The QPOs display both hard and soft lags, as well as near unity coherence in two of the QPO types.

G.S. would like to thank J. Poutanen, J. Homan, and R. Wijnands for helpful discussions.

## REFERENCES

- Bendat, J. & Piersol, A. 1986, *Random Data: Analysis and Measurement Procedures* (New York: Wiley)
- Böttcher, M. & Liang, E. P. 1998, *ApJ*, 506, 281
- Böttcher, M. & Liang, E. P. 1999, *ApJ*, 511, L37
- Cui, W. 1999, *ApJ*, 524, L59
- Cui, W., Zhang, S. N. & Chen, W. 2000, *ApJ*, in press
- Cui, W., Zhang, S. N., Chen, W., & Morgan, E. H. 1999, *ApJ*, 512, L43
- Cui, W., Zhang, S. N., Focke, W., & Swank, J. H. 1997, *ApJ*, 484, 383
- Ford, E. C. & van der Klis, M. 1998, *ApJ*, 506, L39
- Hua, X.-M. & Titarchuk, L. 1996, *ApJ*, 496, 280
- Homan, J., Wijnands, R., van der Klis, M., Belloni, T., van Paradijs, J., Klein-Wolt, M., Fender, R., & Méndez, M. 2000, *ApJ*, submitted (astro-ph/0001163)
- Kazanas, D., Hua, X.-M., & Titarchuk, L. 1997, *ApJ*, 480, 735
- Levine, A. M., Bradt, H., Cui, W., Jernigan, J. G., Morgan, E. H., Remillard, R., Shirey, R. E., & Smith, D. A. 1996, *ApJ*, 469, 33
- Markwardt, C. B., Swank, J. H., & Taam, R. E. 1999, *ApJ*, 513, L37
- Markwardt, C. B., Strohmayer, T. E., & Swank, J. H. 1999, *ApJ*, 512, L125
- Miyamoto, S., Kitamoto, S., Mitsuda, K., & Dotani, T. 1988 *Nature*, 336, 450
- Nowak, M. A., Vaughan, B. A., Wilms, J., Dove, J. B., & Begelman, M. C. 1999, *ApJ*, 510, 874
- Psaltis, D., Belloni, T., & van der Klis, M. 1999, *ApJ*, 520, 262

- Poutanen, J. & Fabian, A. C. 1999, MNRAS, 306, L31
- Remillard, R. A., McClintock, J. E., Sobczak, G. J., Bailyn, C. D., Orosz, J. A., Morgan, E. H., & Levine, A. M. 1999, ApJ, 517, L127
- Smith, D. A. & RXTE/ASM teams 1998, IAU Circ. 7008
- Sobczak, G. J., McClintock, J. E., Remillard, R. A., Levine, A. M., Morgan, E. H., Bailyn, C. D., & Orosz, J. A. 1999, ApJ, 517, L121
- Sobczak, G. J., McClintock, J. E., Remillard, R. A., Cui, W., Levine, A. M., Morgan, E. H., Orosz, J. A., & Bailyn, C. D. 2000a, ApJ, 531, 537
- Sobczak, G. J., McClintock, J. E., Remillard, R. A., Cui, W., Levine, A. M., Morgan, E. H., Orosz, J. A., & Bailyn, C. D. 2000b, ApJ, submitted
- van der Klis, M., Swank, J. H., Zhang, W., Jahoda, K., Morgan, E. H., Lewin, W. H. G., Vaughan, B., & van Paradijs, J. 1996, ApJ, 469, L1
- Vaughan, B. A. & Nowak, M. A. 1997, ApJ, 474, L43
- Wijnands, R., Homan, J., & van der Klis, M. 1999, ApJ, 526, 33

Table 1. Low-Frequency QPO Parameters for XTE J1550–564: Fundamental and Harmonic Frequencies

Obs #	Date (yymmdd)	MJD <sup>a</sup>	Type	QPO Freq. <sup>b</sup> (Hz)	QPO Amp. <sup>c</sup> (% rms)	Q <sup>d</sup>	Phase Lag <sup>e</sup> (radians)	Coherence <sup>f</sup>
2	980908	51064.01	C	0.12	14.7 ± 1.2	1.2	−0.04 ± 0.08	0.99 ± 0.03
...	...	...	...	0.06	6.3 ± 1.5	2.3	0.05 ± 0.12	0.98 ± 0.06
...	...	...	...	0.23	18.7 ± 3.1	0.5	0.04 ± 0.09	0.99 ± 0.04
3	980909	51065.07	C	0.29	16.5 ± 1.3	9.5	−0.02 ± 0.07	0.99 ± 0.03
...	...	...	...	0.16	5.0 ± 1.5	4.8	−0.03 ± 0.12	0.95 ± 0.07
...	...	...	...	0.59	7.1 ± 0.9	7.7	0.07 ± 0.09	0.97 ± 0.05
4	980909	51065.34	C	0.39	14.7 ± 1.5	9.9	−0.02 ± 0.09	0.98 ± 0.04
...	...	...	...	0.78	5.7 ± 1.2	12.1	0.08 ± 0.12	0.95 ± 0.07
5	980910	51066.07	C	0.81	15.4 ± 1.0	7.9	0.05 ± 0.08	0.97 ± 0.05
...	...	...	...	1.6	7.6 ± 0.5	5.5	0.17 ± 0.11	0.90 ± 0.08
6	980910	51066.34	C	1.0	16.2 ± 0.8	8.4	0.04 ± 0.08	0.97 ± 0.04
...	...	...	...	2.1	8.1 ± 0.4	4.7	0.17 ± 0.11	0.90 ± 0.08
7	980911	51067.27	C	1.5	14.1 ± 1.1	12.8	0.04 ± 0.07	0.97 ± 0.04
...	...	...	...	3.1	6.6 ± 0.3	6.8	0.18 ± 0.11	0.80 ± 0.09
8	980912	51068.35	C	2.4	13.6 ± 0.8	14.3	0.02 ± 0.07	0.97 ± 0.04
...	...	...	...	1.3	4.4 ± 0.7	2.5	0.02 ± 0.14	0.78 ± 0.11
...	...	...	...	4.7	5.9 ± 0.3	8.3	0.21 ± 0.12	0.78 ± 0.10
9	980913	51069.27	C	3.3	13.1 ± 0.6	15.3	−0.05 ± 0.07	0.97 ± 0.04
...	...	...	...	1.7	3.5 ± 0.5	3.4	−0.03 ± 0.13	0.78 ± 0.10
...	...	...	...	6.6	5.1 ± 0.2	8.9	0.27 ± 0.13	0.69 ± 0.10
10	980914	51070.13	C	3.2	13.4 ± 0.6	14.7	−0.03 ± 0.06	0.97 ± 0.03
...	...	...	...	1.6	4.2 ± 0.6	1.9	−0.01 ± 0.12	0.80 ± 0.09
...	...	...	...	6.3	5.3 ± 0.2	8.9	0.31 ± 0.12	0.64 ± 0.10
11	980914	51070.27	C	3.2	13.1 ± 0.7	18.7	−0.02 ± 0.07	0.96 ± 0.04
...	...	...	...	6.3	5.1 ± 0.2	11.5	0.28 ± 0.12	0.68 ± 0.10
12	980915	51071.20	C	3.7	13.0 ± 0.4	13.3	−0.06 ± 0.07	0.96 ± 0.04
...	...	...	...	1.8	4.4 ± 0.6	1.7	−0.04 ± 0.14	0.76 ± 0.11
...	...	...	...	7.2	4.8 ± 0.2	10.0	0.28 ± 0.13	0.67 ± 0.11
13	980915	51072.00	C	2.6	14.1 ± 2.8	27.9	0.00 ± 0.08	0.98 ± 0.04
...	...	...	...	1.4	3.4 ± 0.7	5.9	0.00 ± 0.17	0.77 ± 0.13
...	...	...	...	5.1	5.9 ± 0.3	12.6	0.30 ± 0.15	0.75 ± 0.12

Table 1—Continued

Obs #	Date (yyymmdd)	MJD <sup>a</sup>	Type	QPO Freq. <sup>b</sup> (Hz)	QPO Amp. <sup>c</sup> (% rms)	Q <sup>d</sup>	Phase Lag <sup>e</sup> (radians)	Coherence <sup>f</sup>
14	980916	51072.34	C	4.0	12.3 ± 0.4	15.0	−0.07 ± 0.07	0.96 ± 0.04
...	...	...	...	2.0	3.6 ± 0.5	2.5	−0.06 ± 0.13	0.80 ± 0.10
...	...	...	...	7.9	4.3 ± 0.2	10.4	0.32 ± 0.13	0.64 ± 0.11
15	980918	51074.14	C	5.7	9.4 ± 0.3	8.6	−0.16 ± 0.08	0.92 ± 0.05
...	...	...	...	2.8	4.5 ± 0.7	2.1	−0.15 ± 0.12	0.86 ± 0.09
...	...	...	...	11.1	2.6 ± 0.2	4.7	0.04 ± 0.15	0.64 ± 0.13
16 <sup>†,*</sup>	980919	51075.99	?	13.1	1.0 ± 0.1	2.8	−0.92 ± 0.21	0.84 ± 0.23
17 <sup>†</sup>	980920	51076.80	C <sub>2</sub>	7.2	6.6 ± 0.1	5.0	−0.21 ± 0.08	0.86 ± 0.06
...	...	...	...	3.3	4.6 ± 0.3	1.7	−0.27 ± 0.10	0.86 ± 0.07
18 <sup>†,1</sup>	980920	51076.95	C <sub>2</sub>	8.5	4.8 ± 0.1	4.3	−0.25 ± 0.08	0.88 ± 0.06
...	...	...	...	16.9	3.3 ± 0.3	1.0	−0.09 ± 0.16	0.71 ± 0.18
19 <sup>1</sup>	980921	51077.14	C <sub>2</sub>	9.8	3.3 ± 0.1	9.2	−0.32 ± 0.08	0.90 ± 0.05
...	...	...	...	20.1	2.3 ± 0.1	2.0	0.08 ± 0.17	0.71 ± 0.18
20 <sup>1</sup>	980921	51077.21	C <sub>2</sub>	7.1	4.0 ± 0.1	5.4	−0.20 ± 0.07	0.89 ± 0.06
...	...	...	...	3.3	4.8 ± 0.2	1.4	−0.23 ± 0.08	0.92 ± 0.06
21	980921	51077.87	C <sub>2</sub>	5.8	4.8 ± 0.2	11.6	−0.14 ± 0.06	0.88 ± 0.04
...	...	...	...	3.0	4.5 ± 0.4	1.5	−0.19 ± 0.08	0.86 ± 0.06
...	...	...	...	11.4	2.4 ± 0.1	2.3	−0.08 ± 0.11	0.57 ± 0.08
22	980922	51078.13	C	5.4	10.0 ± 0.2	10.7	−0.13 ± 0.07	0.92 ± 0.04
...	...	...	...	2.8	3.1 ± 0.4	3.0	−0.13 ± 0.11	0.85 ± 0.08
...	...	...	...	10.6	3.1 ± 0.1	5.9	0.17 ± 0.13	0.60 ± 0.11
23 <sup>2</sup>	980923	51079.79	C	4.2	12.9 ± 0.4	7.3	−0.02 ± 0.06	0.98 ± 0.03
...	...	...	...	7.9	5.6 ± 0.3	3.4	0.08 ± 0.10	0.90 ± 0.07
24 <sup>2</sup>	980924	51080.08	C	3.9	12.2 ± 0.4	13.6	−0.02 ± 0.06	0.98 ± 0.03
...	...	...	...	1.9	4.1 ± 0.4	2.8	−0.05 ± 0.10	0.91 ± 0.07
...	...	...	...	7.6	4.1 ± 0.2	9.4	0.10 ± 0.08	0.90 ± 0.06
25	980925	51081.06	C	2.9	13.4 ± 0.4	9.8	−0.01 ± 0.06	0.97 ± 0.03
...	...	...	...	1.4	3.9 ± 0.5	3.8	0.02 ± 0.12	0.76 ± 0.10
...	...	...	...	5.7	6.2 ± 0.2	5.3	0.23 ± 0.11	0.73 ± 0.09
26	980926	51082.00	C	2.7	14.0 ± 0.4	10.4	−0.01 ± 0.05	0.97 ± 0.03
...	...	...	...	1.3	5.2 ± 0.7	2.4	0.04 ± 0.11	0.79 ± 0.08
...	...	...	...	5.4	5.7 ± 0.2	7.4	0.22 ± 0.09	0.75 ± 0.08
27	980927	51083.00	C	2.7	14.4 ± 0.4	8.9	−0.02 ± 0.06	0.96 ± 0.04
...	...	...	...	1.4	4.6 ± 0.8	2.9	0.02 ± 0.12	0.80 ± 0.09
...	...	...	...	5.2	6.0 ± 0.2	7.1	0.21 ± 0.11	0.75 ± 0.09

Table 1—Continued

Obs #	Date (yymmdd)	MJD <sup>a</sup>	Type	QPO Freq. <sup>b</sup> (Hz)	QPO Amp. <sup>c</sup> (% rms)	Q <sup>d</sup>	Phase Lag <sup>e</sup> (radians)	Coherence <sup>f</sup>
28	980928	51084.34	C	2.7	14.1 ± 0.5	11.0	−0.01 ± 0.06	0.97 ± 0.03
...	...	...	...	1.4	6.6 ± 0.9	2.2	0.02 ± 0.12	0.78 ± 0.09
...	...	...	...	5.3	5.8 ± 0.2	6.9	0.21 ± 0.10	0.75 ± 0.08
29	980929	51085.27	C	4.1	12.6 ± 0.3	11.1	−0.08 ± 0.06	0.96 ± 0.03
...	...	...	...	2.0	4.7 ± 0.3	2.7	−0.07 ± 0.11	0.82 ± 0.08
...	...	...	...	8.1	4.0 ± 0.2	9.0	0.23 ± 0.11	0.68 ± 0.10
30	980929	51085.92	C	2.9	14.3 ± 0.6	9.5	−0.02 ± 0.08	0.96 ± 0.04
...	...	...	...	1.4	5.2 ± 0.9	3.1	−0.04 ± 0.15	0.77 ± 0.12
...	...	...	...	5.7	4.5 ± 0.4	11.6	0.20 ± 0.13	0.79 ± 0.11
31	980929	51085.99	C	3.0	14.4 ± 0.6	6.5	−0.03 ± 0.07	0.95 ± 0.04
...	...	...	...	1.5	5.8 ± 0.5	2.5	0.02 ± 0.11	0.80 ± 0.09
...	...	...	...	6.0	6.8 ± 0.2	4.0	0.17 ± 0.11	0.75 ± 0.09
32	980930	51086.89	C	3.5	14.0 ± 0.2	8.2	−0.05 ± 0.05	0.96 ± 0.03
...	...	...	...	1.7	6.1 ± 0.2	2.4	−0.00 ± 0.09	0.80 ± 0.07
...	...	...	...	6.9	5.5 ± 0.1	5.8	0.21 ± 0.09	0.74 ± 0.08
33	981001	51087.72	C	3.4	14.2 ± 0.3	8.9	−0.05 ± 0.05	0.96 ± 0.03
...	...	...	...	1.7	5.8 ± 0.3	2.8	0.01 ± 0.10	0.83 ± 0.07
...	...	...	...	6.8	5.8 ± 0.2	5.5	0.19 ± 0.09	0.76 ± 0.08
34	981002	51088.01	C	3.2	14.4 ± 0.4	8.6	−0.05 ± 0.06	0.96 ± 0.03
...	...	...	...	1.6	6.4 ± 0.4	2.3	0.00 ± 0.11	0.81 ± 0.08
...	...	...	...	6.3	6.1 ± 0.2	5.3	0.22 ± 0.10	0.76 ± 0.08
35	981003	51089.01	C	3.0	15.0 ± 0.5	8.2	−0.03 ± 0.07	0.97 ± 0.04
...	...	...	...	1.5	5.9 ± 0.6	3.2	0.00 ± 0.13	0.81 ± 0.10
...	...	...	...	6.0	6.3 ± 0.3	5.3	0.22 ± 0.12	0.79 ± 0.10
36	981004	51090.14	C	3.9	13.3 ± 0.4	10.2	−0.08 ± 0.07	0.96 ± 0.04
...	...	...	...	2.0	5.7 ± 0.3	3.0	−0.05 ± 0.12	0.82 ± 0.09
...	...	...	...	7.8	5.3 ± 0.2	5.7	0.23 ± 0.12	0.71 ± 0.11
37	981004	51090.70	C	3.7	13.7 ± 0.4	9.6	−0.07 ± 0.07	0.96 ± 0.04
...	...	...	...	1.9	6.1 ± 0.3	2.8	−0.05 ± 0.12	0.83 ± 0.09
...	...	...	...	7.4	5.4 ± 0.2	6.0	0.19 ± 0.12	0.76 ± 0.10
38	981005	51091.74	C	5.6	10.0 ± 0.3	11.4	−0.13 ± 0.08	0.92 ± 0.05
...	...	...	...	2.8	4.8 ± 0.3	2.8	−0.13 ± 0.13	0.84 ± 0.10
...	...	...	...	11.0	3.2 ± 0.2	6.6	0.26 ± 0.16	0.67 ± 0.17
39	981007	51093.14	C	6.5	7.5 ± 0.3	11.1	−0.23 ± 0.08	0.89 ± 0.05
...	...	...	...	3.3	4.5 ± 0.3	2.5	−0.23 ± 0.12	0.81 ± 0.09

Table 1—Continued

Obs #	Date (yymmdd)	MJD <sup>a</sup>	Type	QPO Freq. <sup>b</sup> (Hz)	QPO Amp. <sup>c</sup> (% rms)	Q <sup>d</sup>	Phase Lag <sup>e</sup> (radians)	Coherence <sup>f</sup>
...	...	...	...	12.7	2.5 ± 0.1	4.5	0.23 ± 0.16	0.55 ± 0.14
40	981008	51094.14	C	4.3	12.4 ± 0.4	11.1	-0.10 ± 0.07	0.96 ± 0.04
...	...	...	...	2.1	6.2 ± 0.3	3.0	0.00 ± 0.12	0.88 ± 0.09
...	...	...	...	8.6	4.9 ± 0.2	6.0	0.22 ± 0.14	0.78 ± 0.15
41	981008	51094.57	C	5.1	11.3 ± 0.3	11.2	-0.14 ± 0.07	0.95 ± 0.04
...	...	...	...	2.5	6.0 ± 0.2	2.6	-0.10 ± 0.11	0.84 ± 0.09
...	...	...	...	10.1	4.1 ± 0.1	5.9	0.23 ± 0.13	0.72 ± 0.14
42	981009	51095.61	C	4.5	12.1 ± 0.6	12.8	-0.13 ± 0.08	0.96 ± 0.05
...	...	...	...	2.2	6.6 ± 0.5	2.9	-0.04 ± 0.14	0.84 ± 0.11
...	...	...	...	8.9	4.6 ± 0.3	6.4	0.27 ± 0.16	0.71 ± 0.15
43	981010	51096.57	C	5.4	11.7 ± 0.2	4.9	-0.14 ± 0.08	0.90 ± 0.05
...	...	...	...	2.7	7.1 ± 0.6	2.2	-0.11 ± 0.11	0.82 ± 0.08
...	...	...	...	10.0	7.2 ± 0.3	1.6	0.15 ± 0.13	0.60 ± 0.11
44	981011	51097.57	C	4.7	12.0 ± 0.5	10.3	-0.13 ± 0.08	0.95 ± 0.05
...	...	...	...	2.3	6.3 ± 0.4	2.8	-0.10 ± 0.14	0.86 ± 0.10
...	...	...	...	9.4	4.5 ± 0.3	5.9	0.28 ± 0.16	0.68 ± 0.15
45	981011	51097.81	C	4.2	13.5 ± 0.6	9.9	-0.10 ± 0.09	0.95 ± 0.06
...	...	...	...	2.1	6.3 ± 0.6	3.0	-0.04 ± 0.16	0.80 ± 0.12
...	...	...	...	8.4	5.6 ± 0.3	5.3	0.25 ± 0.16	0.78 ± 0.15
46	981012	51098.28	C	5.0	11.6 ± 0.4	10.1	-0.13 ± 0.10	0.94 ± 0.20
...	...	...	...	2.5	6.5 ± 0.3	3.1	-0.11 ± 0.14	0.84 ± 0.23
...	...	...	...	9.9	4.6 ± 0.2	5.2	0.23 ± 0.16	0.79 ± 0.26
47	981013	51099.21	C	4.8	11.5 ± 0.5	11.1	-0.14 ± 0.09	0.94 ± 0.05
...	...	...	...	2.4	6.2 ± 0.4	3.2	-0.09 ± 0.14	0.83 ± 0.11
...	...	...	...	9.7	4.6 ± 0.2	5.5	0.33 ± 0.16	0.73 ± 0.15
48	981013	51099.61	C	5.0	11.7 ± 0.3	9.0	-0.15 ± 0.08	0.94 ± 0.05
...	...	...	...	2.5	6.7 ± 0.3	2.7	-0.05 ± 0.13	0.82 ± 0.09
...	...	...	...	9.9	4.7 ± 0.2	4.8	0.28 ± 0.14	0.79 ± 0.16
49	981014	51100.29	C	6.4	7.6 ± 0.3	10.9	-0.28 ± 0.09	0.89 ± 0.06
...	...	...	...	3.3	5.3 ± 0.3	2.8	-0.15 ± 0.14	0.82 ± 0.11
...	...	...	...	12.9	2.6 ± 0.2	5.5	0.27 ± 0.18	0.57 ± 0.17
50	981015	51101.61	C	6.8	7.0 ± 0.3	6.7	-0.29 ± 0.11	0.84 ± 0.08
...	...	...	...	3.5	4.9 ± 0.3	2.7	-0.23 ± 0.15	0.77 ± 0.12
...	...	...	...	13.5	2.7 ± 0.3	3.7	0.31 ± 0.19	0.67 ± 0.21
51	981015	51101.94	C	6.7	7.0 ± 0.3	9.1	-0.32 ± 0.10	0.88 ± 0.07

Table 1—Continued

Obs #	Date (yyymmdd)	MJD <sup>a</sup>	Type	QPO Freq. <sup>b</sup> (Hz)	QPO Amp. <sup>c</sup> (% rms)	Q <sup>d</sup>	Phase Lag <sup>e</sup> (radians)	Coherence <sup>f</sup>
...	...	...	...	3.5	5.7 ± 0.3	2.6	−0.19 ± 0.14	0.78 ± 0.11
...	...	...	...	13.1	4.4 ± 0.4	1.9	0.33 ± 0.18	0.51 ± 0.15
52 <sup>†</sup>	981020	51106.95	B	5.5	3.8 ± 0.1	8.9	0.19 ± 0.12	1.01 ± 0.09
...	...	...	...	2.5	1.1 ± 0.2	3.0	−0.80 ± 0.46	0.27 ± 0.53
...	...	...	...	10.6	2.0 ± 0.1	4.8	−0.47 ± 0.22	1.11 ± 0.31
53 <sup>†</sup>	981022	51108.08	B	5.4	4.1 ± 0.0	8.6	0.26 ± 0.07	0.98 ± 0.05
...	...	...	...	2.8	1.3 ± 0.1	5.7	−0.33 ± 0.20	0.85 ± 0.34
...	...	...	...	10.5	2.2 ± 0.0	5.2	−0.43 ± 0.11	0.96 ± 0.13
54 <sup>†</sup>	981023	51109.74	B	4.9	4.0 ± 0.1	11.2	0.13 ± 0.11	0.97 ± 0.08
...	...	...	...	2.6	0.5 ± 0.2	6.6	−1.43 ± 0.91	0.43 ± 1
...	...	...	...	9.8	1.9 ± 0.1	5.6	−0.38 ± 0.22	1.14 ± 0.33
59 <sup>†</sup>	981029	51115.28	A	6.8	2.8 ± 0.2	1.8	−1.18 ± 0.36	0.0 ± 1
151	990302	51239.08	?	18.1	0.5 ± 0.1	17.6	−1.04 ± 0.39	0.49 ± 0.56
153 <sup>†</sup>	990304	51241.83	A	5.9	2.9 ± 0.1	3.0	−0.63 ± 0.23	0.72 ± 0.33
154 <sup>†</sup>	993005	51242.51	A	5.7	2.4 ± 0.1	2.5	−1.38 ± 0.31	0.62 ± 1
156 <sup>†</sup>	990308	51245.35	B	6.3	3.6 ± 0.1	11.7	0.37 ± 0.10	0.96 ± 0.08
...	...	...	...	3.1	1.8 ± 0.1	3.6	−0.45 ± 0.27	1.20 ± 1
...	...	...	...	12.3	1.7 ± 0.1	6.4	−0.43 ± 0.18	0.98 ± 0.22
158 <sup>†</sup>	990310	51247.98	B	6.1	3.7 ± 0.1	9.9	0.33 ± 0.10	0.94 ± 0.07
...	...	...	...	3.1	2.0 ± 0.1	4.5	−0.51 ± 0.21	0.94 ± 0.31
...	...	...	...	12.0	1.8 ± 0.1	5.6	−0.41 ± 0.17	0.94 ± 0.20
159 <sup>†</sup>	990311	51248.09	B	5.9	3.7 ± 0.1	11.0	0.18 ± 0.12	0.97 ± 0.09
...	...	...	...	2.7	1.4 ± 0.2	2.4	−0.82 ± 0.48	0.0 ± 1
...	...	...	...	11.8	1.5 ± 0.1	7.1	−0.44 ± 0.24	1.16 ± 0.35
160 <sup>†</sup>	990312	51249.40	B	6.2	3.8 ± 0.1	9.4	0.38 ± 0.13	0.99 ± 0.12
...	...	...	...	3.1	2.8 ± 0.1	5.3	−0.27 ± 0.23	0.86 ± 0.27
...	...	...	...	11.9	1.9 ± 0.1	5.7	−0.48 ± 0.24	1.18 ± 0.37
161 <sup>†</sup>	990313	51250.69	C	6.7	6.5 ± 0.3	8.8	−0.36 ± 0.12	0.82 ± 0.10
...	...	...	...	3.4	5.1 ± 0.3	2.7	−0.14 ± 0.17	0.71 ± 0.16
...	...	...	...	13.6	1.9 ± 0.3	7.9	0.31 ± 0.22	0.59 ± 0.23
162 <sup>†</sup>	990316	51253.22	B	5.5	4.2 ± 0.1	9.6	0.28 ± 0.12	0.98 ± 0.10
...	...	...	...	2.8	1.7 ± 0.1	6.3	−0.24 ± 0.30	1.33 ± 1
...	...	...	...	10.6	2.3 ± 0.1	5.0	−0.39 ± 0.22	1.37 ± 0.41
163 <sup>†</sup>	990317	51254.09	B	6.2	4.4 ± 0.2	4.1	0.14 ± 0.16	0.77 ± 0.14
...	...	...	...	3.2	3.3 ± 0.2	3.1	−0.35 ± 0.25	0.41 ± 0.17

Table 1—Continued

Obs #	Date (yymmdd)	MJD <sup>a</sup>	Type	QPO Freq. <sup>b</sup> (Hz)	QPO Amp. <sup>c</sup> (% rms)	Q <sup>d</sup>	Phase Lag <sup>e</sup> (radians)	Coherence <sup>f</sup>
164 <sup>†</sup>	990318	51255.09	A	6.2	2.4 ± 0.2	1.9	−1.01 ± 0.34	0.12 ± 1
...	...	...	...	13.6	1.8 ± 0.3	2.1	−0.02 ± 0.30	0.0 ± 1

<sup>a</sup>Start of observation,  $MJD = JD - 2,400,000.5$ .

<sup>b</sup>The statistical errors in the QPO centroid frequency are < 1% at the 95% confidence level.

<sup>c</sup>The integrated fractional rms amplitude of the QPO is the square root of the integrated power in the QPO feature, expressed as a fraction of the mean count rate. Errors are given at the 95% confidence level.

<sup>d</sup>Q = QPO Frequency/FWHM

<sup>e</sup>Phase lag between 2–13 keV and 13–30 keV bands. A positive value corresponds to a hard lag. Errors are given at the  $1\sigma$  confidence level.

<sup>f</sup>Errors are given at the  $1\sigma$  confidence level.

<sup>†</sup>Indicates observations during which high-frequency (100–285 Hz) QPOs are also observed (Remillard et al. 1999; Homan et al. 2000; Remillard, private communication).

\*6.8 Crab flare (see Fig. 1 in Sobczak et al. 1999, 2000b).

<sup>1</sup>Soft band: channels 0–30, 2–11.3 keV; Hard band: channels 31–49, 11.3–18.3 keV (see §2)

<sup>2</sup>Soft band: channels 0–17, 2–6.5 keV; Hard band: channels 18–249, 6.5–30 keV, effectively (see §2)

Table 2. Summary of QPO Types

Property	Type A	Type B	Type C
Frequency (Hz)	$\sim 6$	5–6	0.1–10
Amplitude (%rms)	3–4	$\sim 4$	3–16
Q <sup>a</sup>	$\sim 2$ –4	$\sim 4$	$\gtrsim 10$
Phase Lag (rad.)	–0.6 to –1.4	0 to 0.4	0.05 to –0.4
Sub-Harmonic	...	soft	soft
1st Harmonic	soft	soft	hard
Coherence	$< 0.5$	$\sim 1$	$\sim 0.9$
HFQPOs	All	All	3/50

<sup>a</sup>Q = QPO frequency/FWHM

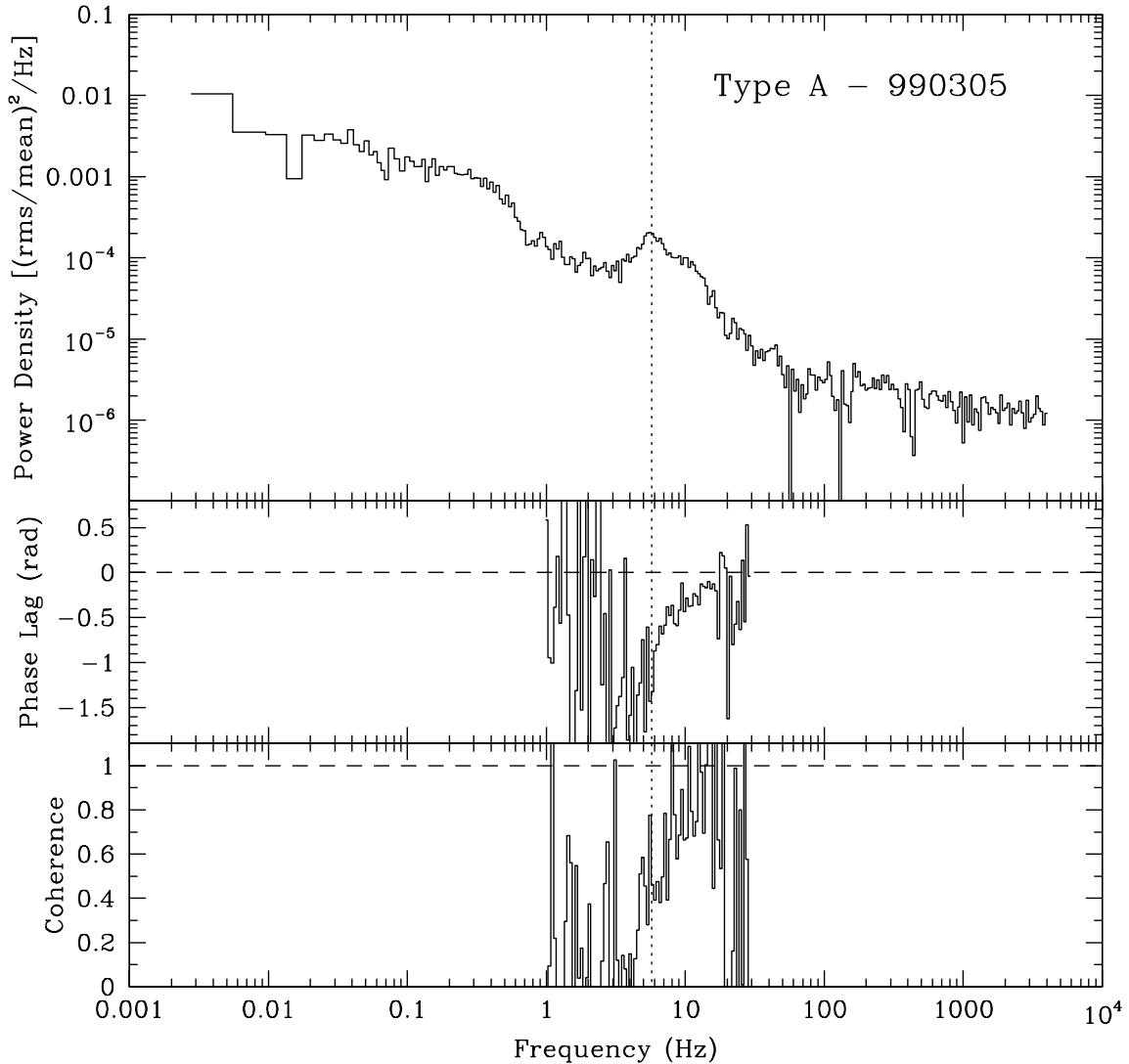


Fig. 1.— Characteristic power spectrum (top), phase lag spectrum (middle), and coherence function (bottom) for Type A QPO behavior (see text for details). The phase lag and coherence are computed between the 2–13 keV and 13–30 keV bands, with a positive phase lag representing a hard lag. For this observation there are  $\sim 15300$  c/s in the 2–13 keV band and  $\sim 600$  c/s in the 13–30 keV band.

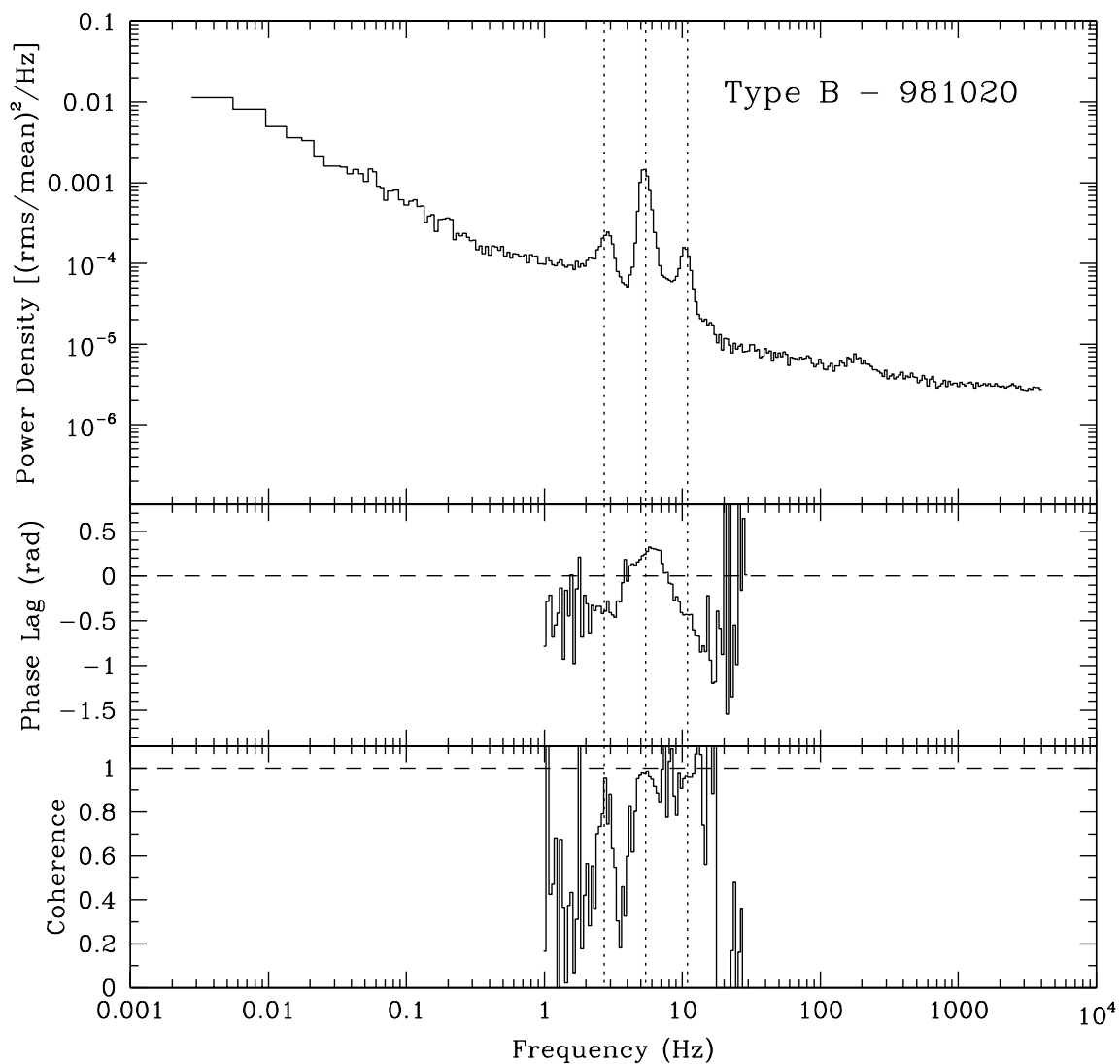


Fig. 2.— Characteristic power spectrum (top), phase lag spectrum (middle), and coherence function (bottom) for Type B QPO behavior (see text for details). For this observation there are  $\sim 18200$  c/s in the 2–13 keV band and  $\sim 1100$  c/s in the 13–30 keV band.

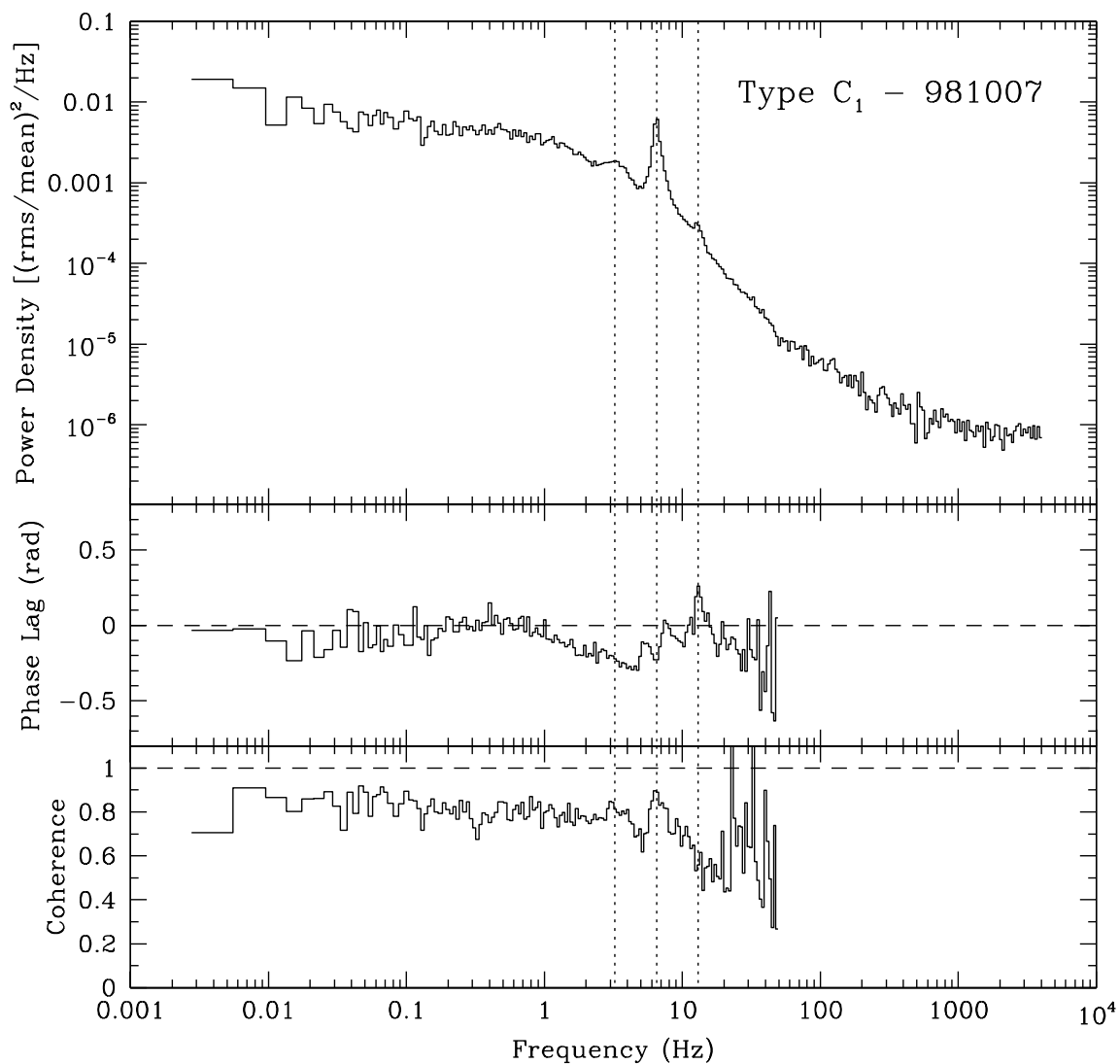


Fig. 3.— Characteristic power spectrum (top), phase lag spectrum (middle), and coherence function (bottom) for Type C QPO behavior (see text for details). For this observation there are  $\sim 19000$  c/s in the 2–13 keV band and  $\sim 1500$  c/s in the 13–30 keV band.

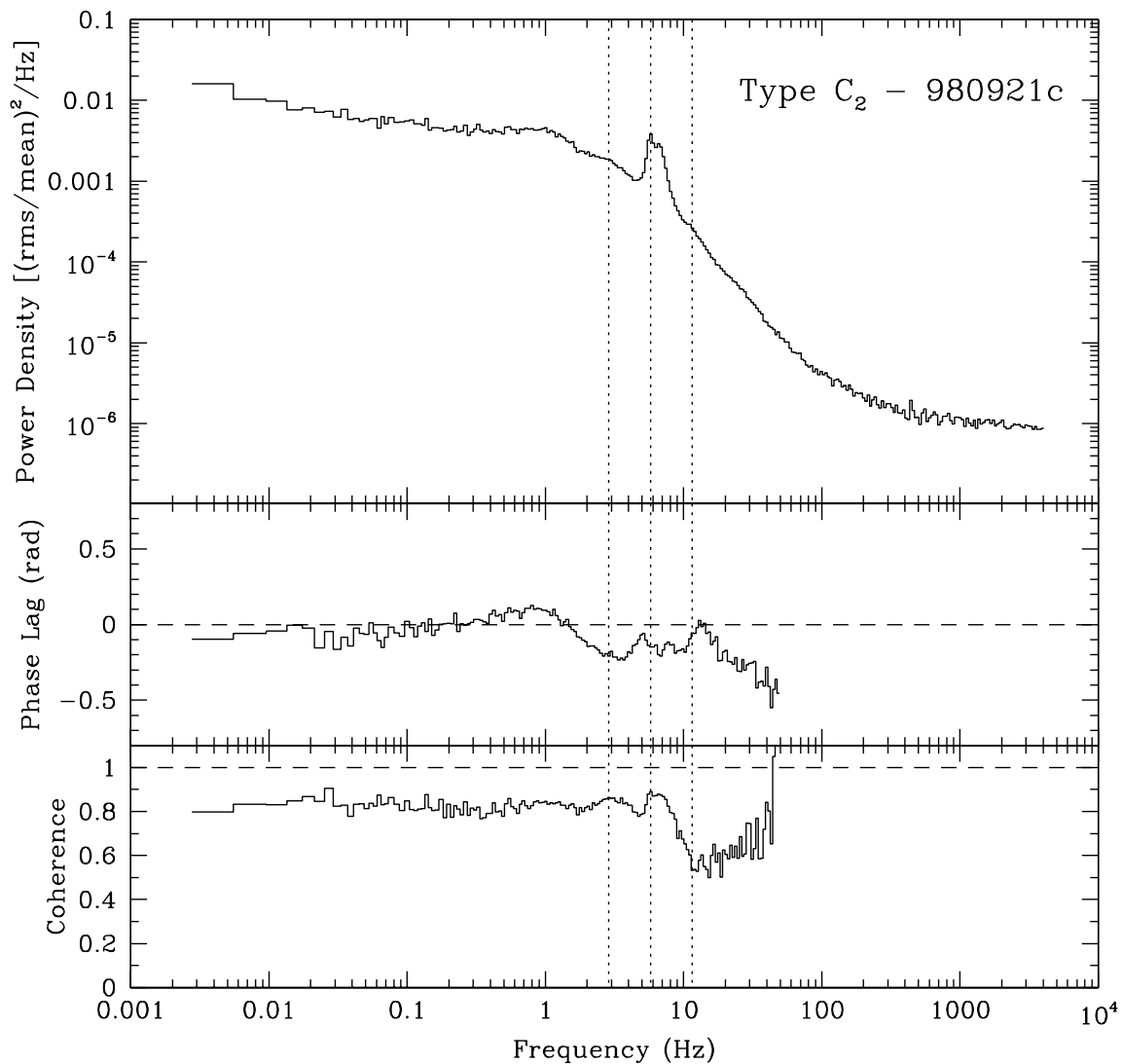


Fig. 4.— Characteristic power spectrum (top), phase lag spectrum (middle), and coherence function (bottom) for Type  $C_2$  QPO behavior (see text for details). For this observation there are  $\sim 27000$  c/s in the 2–13 keV band and  $\sim 1900$  c/s in the 13–30 keV band.

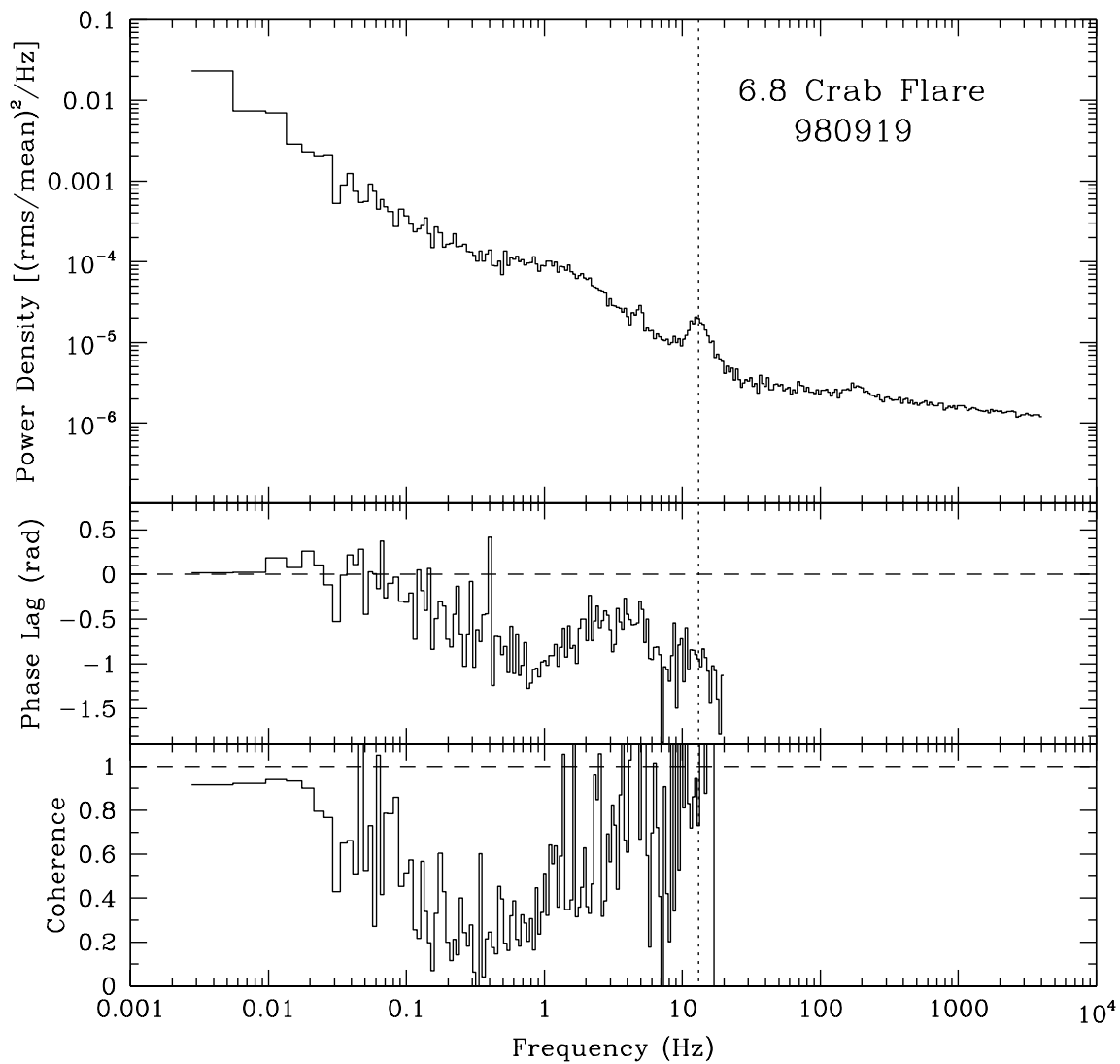


Fig. 5.— Power spectrum (top), phase lag spectrum (middle), and coherence function (bottom) for 6.8 Crab flare on 19 September 1998, which does not fit the type A, B, C classification (see text for details). For this observation there are  $\sim 63000$  c/s in the 2–13 keV band and  $\sim 4100$  c/s in the 13–30 keV band.

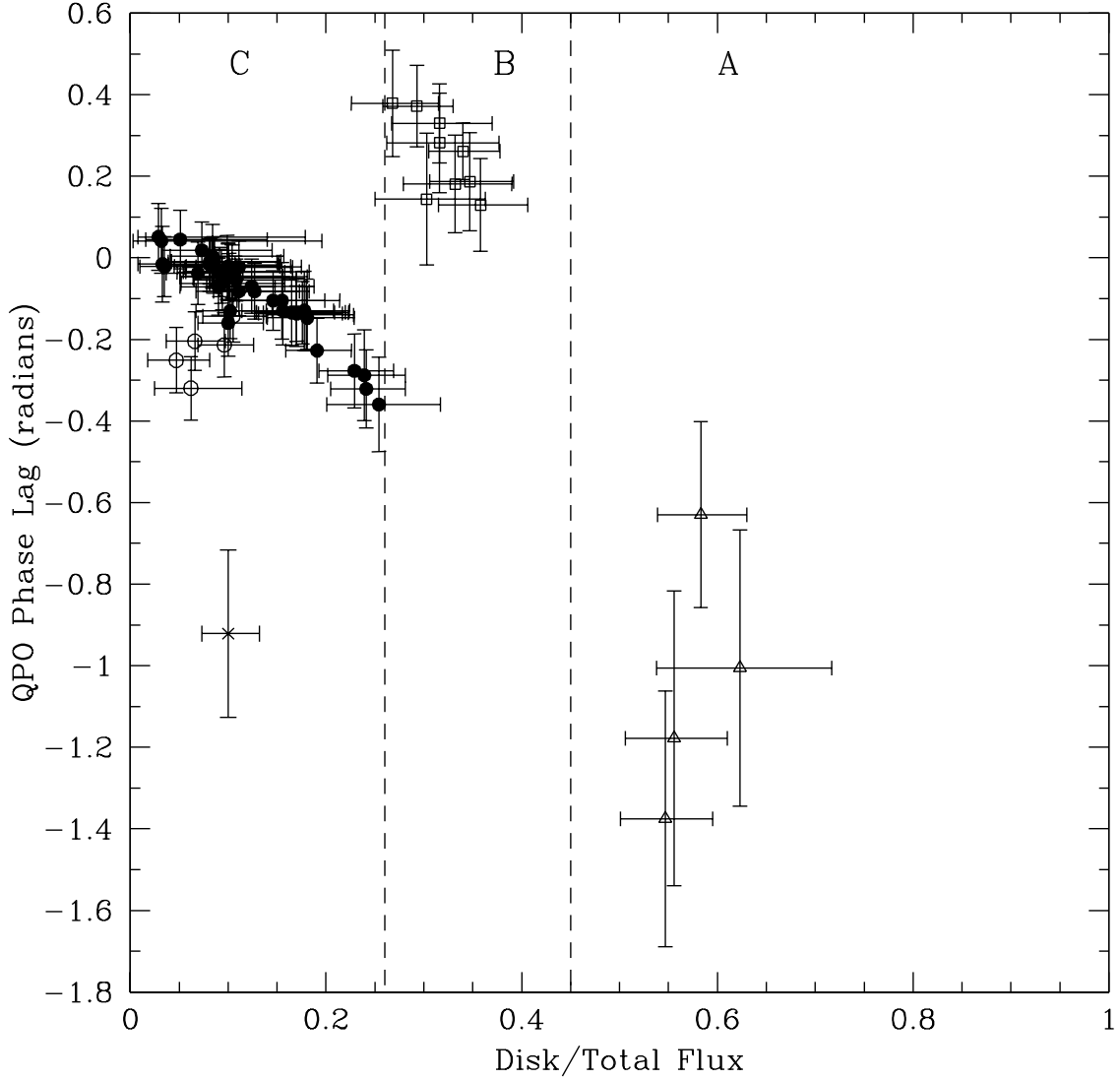


Fig. 6.— Fundamental QPO phase lag vs. the relative contribution of the disk component ( $1 - \text{power-law component}$ ) relative to the total observed flux from 2–20 keV. Flux data obtained from Sobczak et al. (2000b). The observation which took place during the 6.8 Crab flare on 19 September 1998 is represented by the symbol ‘x’. Type C<sub>2</sub> observations are plotted with open circles.

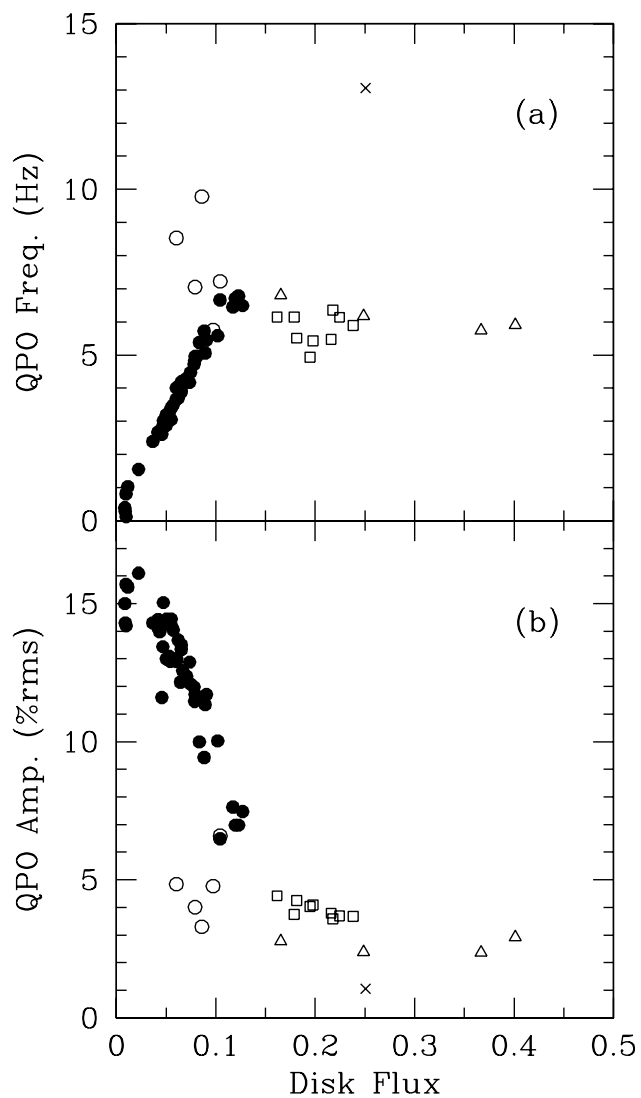


Fig. 7.— (a) QPO frequency and (b) QPO integrated rms amplitude vs. the unabsorbed 2–20 keV disk flux in units of  $10^{-7}$  erg  $s^{-1}$   $cm^{-2}$ . The fundamental types of QPO behavior are plotted as follows: Type A – open triangles, Type B – open squares, Type C<sub>1</sub> – filled circles, Type C<sub>2</sub> – open circles, and the 6.8 Crab flare – ‘x’. The error bars are not shown here, but are comparable to the symbol size for the QPO frequency and amplitude, and are approximately  $\pm 0.02$  in the given units for disk flux.

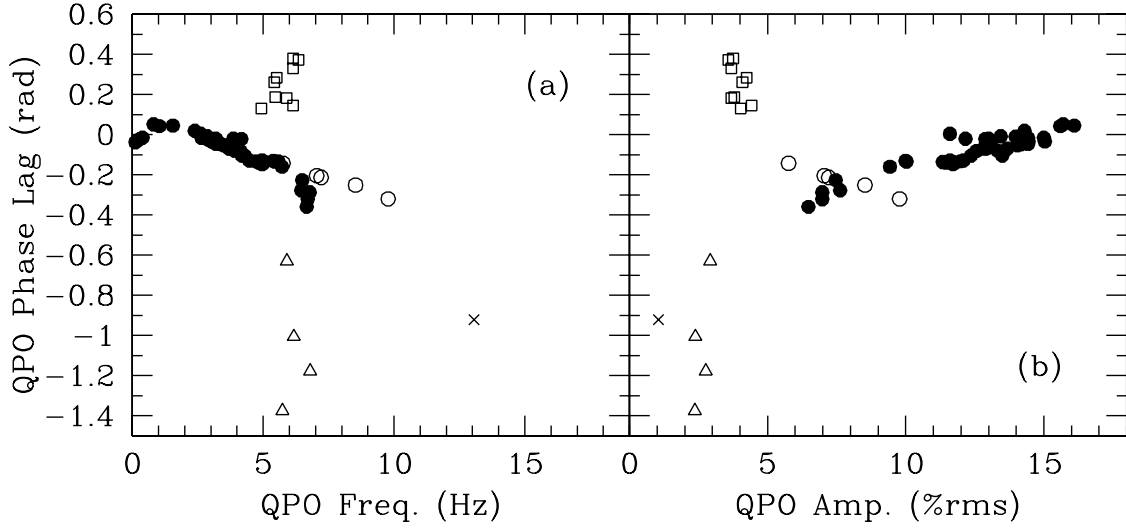


Fig. 8.— Fundamental QPO phase lag vs. (a) frequency and (b) integrated rms amplitude. The plotting symbols are the same as in Figure 7. The error bars are not shown so that the QPO types are easier to discern.